Tension-compression fatigue behaviors of uniform and bimodal carbon nanotube/Al-Cu-Mg composites

K. Ma, X.N. Li, J.F. Zhang, Z.Y. Liu [*], B.L. Xiao [*], Z.Y. Ma

Shi-changxu Innovation Center for Advanced Materials, Institute of Metal Research, Chinese Academy of Science, 72 Wenhua Road, Shenyang 110016, China

ABSTRACT

By introducing the ductile-zones (DZs) without carbon nanotubes (CNTs) into the brittle-zones (BZs) containing CNTs, constructing the bimodal structure, can effectively improve the toughness of CNT reinforced Al (CNT/Al) composites. However, to be applied in the field of aerospace, CNT/Al composites will be required to have high toughness, as well as high fatigue strength. At the present study, the fatigue behaviors of uniform and bimodal CNT/Al composites under the tension-compression state with the stress ratio of −1 were investigated. It was found that CNT rich zones could keep grains stable after the fatigue loading. However, for the bimodal CNT/Al composites, the preferential local deformation occurred in the DZs, which resulted in much lower fatigue strength as compared to the uniform composite. By reducing the grain size of DZs to ultra-fine grain (UFG) level, the large number of grain boundaries within the DZs hindered the directional movement of slip bands, which significantly enhanced the fatigue strength and achieved a higher toughness of bimodal CNT/Al composites. This discovery provides a new strategy for the preparation of high performance CNT/Al composites, and the bimodal CNT/Al composite with UFG DZs is expected to be applied in the aerospace field.

1. Introduction

Adding carbon nanotubes (CNTs) into Al matrix, and obtaining the CNT reinforced Al matrix (CNT/Al) composites will effectively improve the strength and modulus of Al matrix, while keep a good machinability [1–8]. However, CNTs have a strong pinning effect on grain boundaries, which leads to the very small grains and low ductility of CNT/Al composites [9–11]. Developing the bimodal structure by introducing the ductile-zones (DZs) without reinforcements into the brittle-zones (BZs) containing reinforcements is an effective solution to break the bottleneck of low ductility of composites [12–18]. For example, Liu et al. [12] found that the bimodal CNT/Al-Cu-Mg composite exhibited twice the elongation as the uniform CNT/Al-Cu-Mg composite. The improved ductility could be owing to the relief of deformation localization. Besides, geometrically necessary dislocations nucleated at the boundaries between the BZs and DZs, which led to an extra-strengthening effect, and the ultimate tensile strength of the bimodal CNT/Al composite could be maintained at a high level.

As an important service performance, the fatigue behavior is essential for engineering application [19]. However, there were nearly no investigations on the fatigue behaviors of bimodal composites.

According to the traditional views, the fatigue cracks are preferentially nucleated in the inhomogeneous microstructure, and the bimodal structure will deteriorate the fatigue properties [20–24]. For example, Nelson et al. [23] investigated the fatigue behaviors of bimodal Al alloys and found that the microcracks were easier to form in the coarse grain (CG) zones, and the fatigue life decreased with increasing the fraction of the CG zones.

Recently, it was found that the fatigue properties of bimodal materials could be optimized through adjusting the bimodal structure parameters [25–28]. In our previous investigation, the bimodal CNT/Al composite containing the ultra-fine grain (UFG) DZs had the higher tension-tension fatigue strength than that of the uniform CNT/Al composite [28]. The improved fatigue strength attributed to the following two points. First, the UFGs in DZs significantly relaxed the local deformation in the DZs, which inhibited the preferential local damage. Second, the UFGs within the DZs decreased the incongruity of deformation between the BZs and DZs. Therefore, refining the grains in DZs could be a good way to optimize the fatigue behaviors of the bimodal composites.

It should be mentioned that, not only the microstructure, but also the fatigue test condition would affect the fatigue life [29,30]. Some engineering components would be subjected to cyclic tension-compression

---

loading in service, and it had also been widely demonstrated that the tension-compression fatigue strength of materials exhibited more deleterious as compared to the tension-tension fatigue [31–34]. For example, Liu et al. [33] found that the tension-compression fatigue strength with the stress ratio of −1 of Ti–6Al–4 V alloy decreased about 50% as compared to that under the tension-tension condition with the stress ratio of 0.5. The decreased tension-compression fatigue strength could attribute to its larger stress amplitude. Although the fatigue behaviors of the uniform and bimodal CNT/Al composites under tension-tension state have been investigated [28], the tension-compression fatigue behaviors are still unclear.

In this study, the tension-compression fatigue properties of the uniform and two bimodal CNT/Al composites with CGs and UFGs in the DZs with the stress ratio of −1 were tested. The corresponding microstructure evolutions were analyzed. The aim is to (a) evaluate the tension-compression fatigue properties of uniform and bimodal CNT/Al composites, and (b) clarify the damage mechanism of the bimodal composites under the tension-compression fatigue condition.

2. Experimental materials and methods

At the present investigation, the CNT/Al-Cu-Mg composites were fabricated through powder metallurgy route. Fig. 1 shows the microstructures of raw powders. The CNTs (~98% purity) with the outer diameter of 10–20 nm and the length of ~5 μm were fabricated by chemical vapor deposition in Tsinghua University (Fig. 1a). Atomized 2009Al powders with the element content of Al-4 wt% Cu-1.5 wt% Mg had an approximately 10 μm powder diameters (Fig. 1b). The 3 vol% CNT/2009Al composite powders (Fig. 1c) were fabricated by milling CNTs and atomized 2009Al powders, and the milling procedure can be seen as follows:

(1) Pour 3 vol% CNTs and as-received 2009Al powder into an attritor containing steel balls, with a ball to powder ratio of 15:1.

(2) Add 2 wt% stearic acid into the mixing powders to prevent premature welding of powders.

(3) Start the ball milling machine with the rotation rate of 250 rpm for 10 h.

In order to obtain the bimodal composites with different bimodal structures, the high energy ball milling (HEBM) was used to adjust the 2009 Al powder morphology. The HEBM process was a little different from that of the ball milled CNT/2009Al composite powders, no CNTs were added and the milling time was decreased to 4 h. The 2009Al powders after HEBM can be seen in Fig. 1d.

Then the atomized and milled 2009Al powders were respectively mixed with 75 wt% CNT/2009Al composite powders in a mixer with the rotation rate of 50 rpm for 6 h. Therefore, two bimodal composite powders with 2.25 vol% CNT were fabricated. Pour the as mixed two bimodal composite powders into two barrel moulds, respectively. Hot press the composite powders under a vacuum with the pressure of 50 MPa at 540 °C. Then the billets were subjected to extrusion deformation at 470 °C with the extrusion ratio of 16:1. T4 heat treatment was applied on the extruded bars with the solution treatment at 500 °C for 2 h, quenched into water and naturally aged at least 96 h. For simplification, the bimodal composite obtained by introducing the atomized 2009Al powders was abbreviated as Bimodal-CG DZ, while the bimodal composite by introducing the as milled 2009Al powders was abbreviated as Bimodal-UFG DZ.

For a comparison, the uniform CNT/2009Al composite without introducing extra matrix powders was fabricated. The uniform CNT/2009Al composite had the same total content of CNT (2.25 vol%) as the bimodal CNT/2009Al composites, and it was abbreviated as Uniform composite.

The element compositions were measured with a Icap Q mass spectrometer. Tensile and fatigue testing specimens were machined from the extruded bars with the axis along the extrusion elongation direction. The detailed tensile testing methods and results had been reported in Ref. [28]. The fatigue testing specimens had the measured diameter of 6
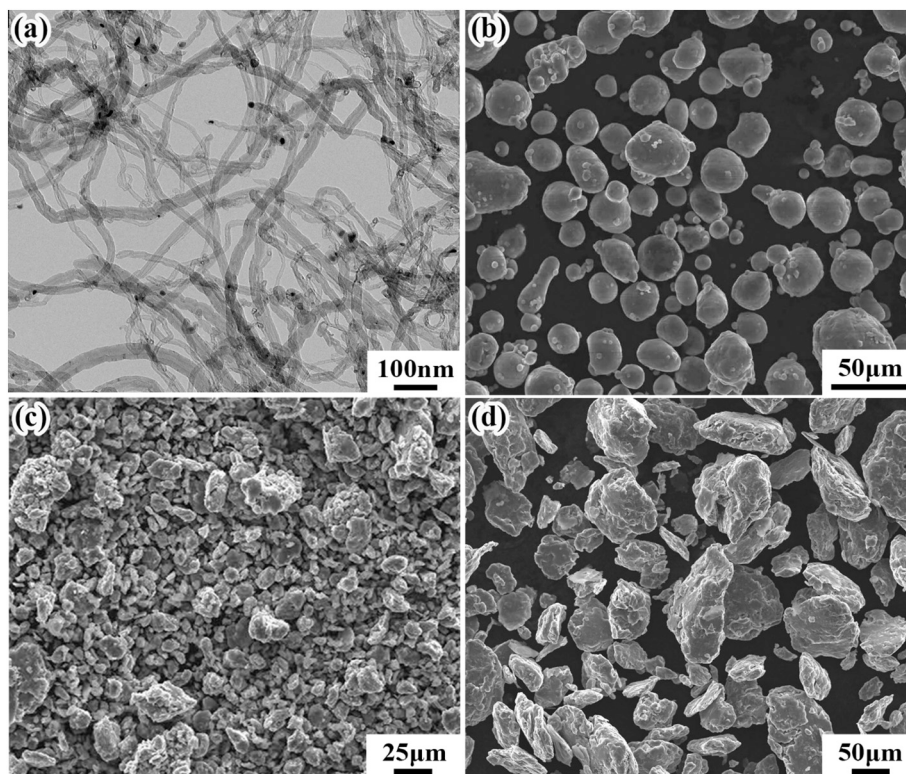
Fig. 1. The raw powder microstructures of: (a) CNT, (b) atomized 2009Al, (c) ball milled 3 vol% CNT/2009Al composite and (d) ball milled 2009Al.

mm and the length of 10 mm. Fatigue tests were carried on by using Instron 8801 tester with the stress ratio of R = -1 (R is the ratio of the minimum applied stress to the maximum applied stresses) and the frequency of 20 Hz at room temperature. Vickers hardness of the BZs and DZs before and after fatigue testing was measured in NG-1000 CCD microhardness test machine, respectively. Optical microscopy (OM; Zeiss Axiovert 200 MAT), scanning electron microscopy (SEM; JSM-6480LV) and transmission electron microscopy (TEM; JEM-2100) were used to observe the microstructures. The TEM sample preparation process is as follows. Cut the foil plane with the thickness of about 0.5 mm from the composite block. Grind the foils and decrease the foil thickness to 60 μm. Punch the thin foils to disks with a diameter of 3 mm, and dimple them to a minimum thickness of 20 μm. Finally, use the Gatan Model 691 ion milling system to thin the foils.

3. Results and discussion

3.1. Initial microstructures

The chemical compositions are shown in Table 1. It can be found that all the three composites had nearly the same element composition. The OM images of the two bimodal composites are shown in Fig. 2, in which, the bright color regions were the DZs, while the dark grey regions were the BZs due to the higher susceptibility of high fraction of grain and phase boundaries to chemical etching. As the result of rheological effect during extrusion, the DZs had a band morphology. For the Bimodal-CG DZ, the DZ bands were thin with the average DZ width of 2.6 μm (Fig. 2a). For the Bimodal-UFG DZ, the DZ bands were much wider with the average DZ width of 6.6 μm (Fig. 2b). The wider DZ band of the Bimodal-UFG DZ could mainly attributed to the much larger size of the milled 2009Al powders.

The TEM images of the Uniform, Bimodal-CG DZ and Bimodal-UFG DZ are shown in Fig. 3. For the Uniform composite, it had the very small grains of only about 200 nm (Fig. 3a), and CNTs (indicated by black arrows in Fig. 3b) were uniformly and singly distributed in the matrix. For the two bimodal composites, DZs free of CNTs were observed to be embedded in the CNT rich zones. For the Bimodal-CG DZ, it had the larger grains in the DZs and the grain width reached to 1–2 μm (Fig. 3c). For the Bimodal-UFG DZ, it had small grains within the DZs and the average grain size was about 500 nm (Fig. 3d). The refined grains in the DZs could be owing to the severe plastic deformation of the milled 2009Al powders during the HEBM process.

3.2. Fatigue properties

Fig. 4a shows the stress amplitude versus the number of cycles-to-failure (S-N curves) of the three CNT/2009Al composites, where the arrows indicate the specimens that did not fail. It can be seen that with increasing the applied stress, the fatigue life decreased. At the same level cyclic loading, the Uniform composite could go through the longer fatigue life as compared to the other two bimodal composites, which indicates that the fatigue performance of the Uniform composite was better. When N_f reaches to approximately 10^7, the corresponding max stress was determined as fatigue strength σ_{FS} [35]. Generally, there is a strong dependence between fatigue strength and tensile strength σ_{TS} [36]. The ratio of σ_{FS} to σ_{TS} can be given as following [37]:

$$m = \sigma_{FS}/\sigma_{TS} \tag{1}$$

Table 1
Chemical compositions of the experimental materials (wt%).

Material	Cu	Mg	Si	Fe	Al
Uniform composite	4.35	1.43	0.05	0.11	Bal.
Bimodal-CG DZ	4.32	1.44	0.06	0.11	Bal.
Bimodal-UFG DZ	4.33	1.42	0.06	0.11	Bal.

According to the fatigue data of many metal materials such as Fe, Cu, and Al alloys, *m* values are estimated to be 0.4 to 0.6 [35,38]. Adding CNTs to the Al alloy matrix, *m* can be further improved. For example, Liao et al. [39] reported that *m* of CNT/Al composite tested at R = 0.1was varied from 0.56 to 0.63. Shin et al. [37] reported that *m* of CNT/2024Al composite tested at R = - 0.5 was varied from 0.60 to 0.78.

Fatigue properties of σ_{FS} and *m* for the present three composites can be seen in Fig. 4b, and Table 2 shows all the tensile and fatigue properties. It can be found that the two bimodal composites had the lower yield strength (YS) than the Uniform composite, but the elongation (El) was improved. Especially for the Bimodal-UFG DZ, its ultimate tensile strength (UTS) was even higher than the Uniform composite, which exhibited a better toughening effect. For the fatigue properties, all *m* values of the three composites were much lower than that reported in Ref. [28] with *R* = 0.1. This was mainly because that the present materials tested at a lower stress ratio of R = - 1 had a larger stress amplitude as compared to that tested at a higher R with the same max stress. By comparing the three composites, it can be known that the Uniform composite had the highest σ_{FS} and *m* among the three composites, which means that the Uniform composite had a better tension-compression fatigue properties than that of the bimodal composites. By comparing the two bimodal composites, it can be seen the Bimodal-UFG DZ had the same *m* with the Bimodal-CG DZ, but the σ_{FS} of the Bimodal-UFG DZ was higher than that of the Bimodal-CG DZ. This means that the Bimodal-UFG DZ had the better tension-compression fatigue behaviors as compared to the Bimodal-CG DZ.

3.3. Fractograph

Fig. 5 shows the fractograph of the three composites after tension-compression fatigue test. From the macro morphologies, it can be found that all the three composite fracture surfaces including four regions, i.e., the fatigue crack nucleation region (Region I), smooth region (Region II), radial region (Region III) and shear lip region (Region IV). The nucleation region is the initial position where the fatigue crack source formed, and then the fatigue crack will expand to the smooth region. With the increase of fatigue cycles, the crack expands rapidly and forms the radial region. In the last cycle before the specimen is disconnected, the specimen tears directly to form the tear lip region. For high cycle fatigue, most of the life is in the stage of crack nucleation, followed by the stage of small crack propagation (forming the smooth region). Therefore, the fracture morphologies of fatigue crack nucleation regions and smooth regions are mainly studied at the present investigation. Therefore, Fig. 5 only provides the magnified photos of fatigue crack nucleation regions and smooth regions. The magnified radial regions and shear lip regions can be seen in Fig. S1.

The fatigue crack nucleation regions of the Uniform composite and Bimodal-UFG DZ were at the specimen surfaces, but the fatigue crack nucleation region of the Bimodal-CG was at the area with a little farther away from the specimen surface (Fig.5a, d and g). Further, the two bimodal composites had the larger smooth regions and smaller radial regions than that in the Uniform composite, which was mainly because that the bimodal structures could reduce the crack sensitivity, and the rapid tearing during the crack propagation could be delayed.

The magnified crack nucleation regions show the crack initiation characteristics. For the Uniform composite, the fatigue crack nucleated at the gap invaded from the surface of the specimen (as indicated by the arrow in Fig. 5b). For the Bimodal-CG DZ, the fatigue crack nucleated at the internal defect, and formed a so called "fish eye" pattern (Fig. 5e). For the Bimodal-UFG DZ, the sliding steps at the surface of the specimen induced the crack nucleation, (as shown by the arrow in Fig. 5h).

The fatigue crack nucleated at the specimen surface had been widely reported, which was mainly because the invading and extruding effect promoted the fatigue defects preferentially initiated at the specimen surface [33,40]. For the Bimodal-CG DZ, the crack nucleation region transferred to the inside of the specimen, which could be owing to that
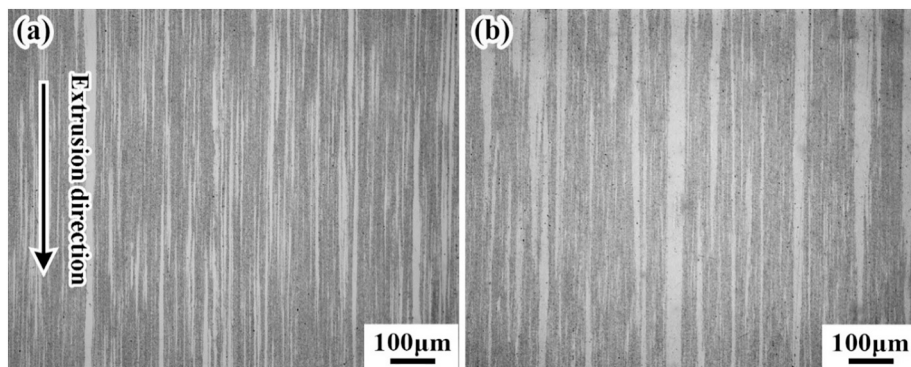
Fig. 2. OM images of: (a) Bimodal-CG DZ and (b) Bimodal-UFG DZ.
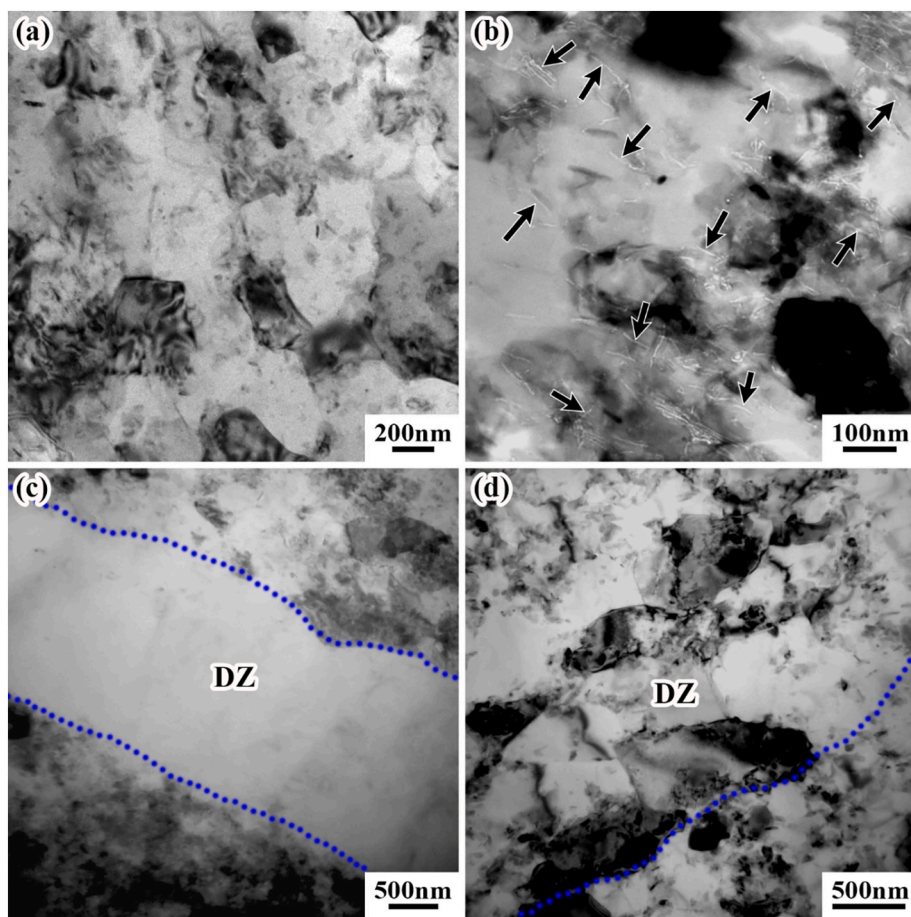
Fig. 3. TEM images of: (a)(b) Uniform composite, (c) Bimodal-CG DZ and (d) Bimodal-UFG DZ (Blue lines are the boundaries between the BZs and DZs). (For interpretation of the references to color in this figure legend, the reader is referred to the web version of this article.)

the CGs on the surface of the specimen will be refined during the turning process, so as to improve the strength of DZs on the specimen surface. The inter low-strength CG DZ was easier to damage than other regions, and the internal damage was formed preferentially.

All the smooth regions of the three composites show that there were no obvious fatigue striations. The dimples of the Uniform composite were small (Fig. 5c), while the Bimodal-CG DZ and Bimodal-UFG DZ had the larger dimples, which indicates more plastic deformation accumulated in the bimodal composites before fracture (Fig. 5f and i). Further, there were some tear ridges in the Bimodal-CG DZ (indicated by blue arrows in Fig. 5f). According to the previous investigations, the tear ridges were caused by grain tearing in the CG DZs [28]. Because there

was a large strength difference between the BZs and DZs, the uncoordinated deformation would be formed at the boundaries between the two zones, which would induce many micro-cracks forming at the edges of the tear ridges (marked by red circles in Fig. 5f). By observing the Fig. 5i, no tear ridges were found. This was because that the grain size difference between the UFG DZs and BZs was decreased, and the grain tearing phenomenon became weaker. However, because the UFG DZs still had the larger grains than the BZs, and with the difference of CNT content between the UFG DZs and BZs, the stress concentration at the boundaries between the two zones still existed. Therefore, micro-cracks could still be observed within the Bimodal-UFG DZ (marked by red circles in Fig. 5i).

K. Ma et al.

Materials Characterization 192 (2022) 112193
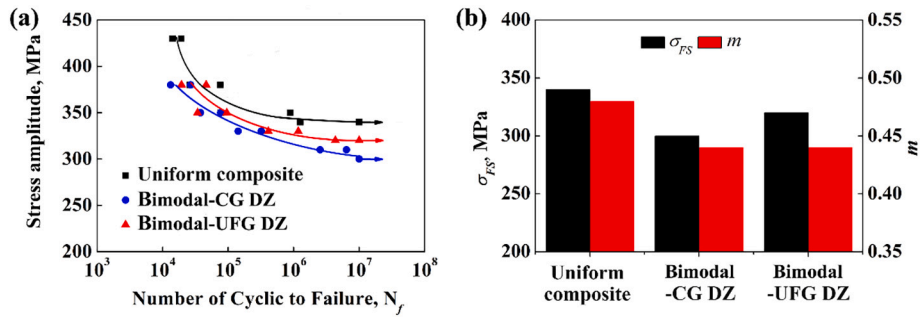
Fig. 4. Tension-compression fatigue properties of uniform and bimodal composites: (a) S-N curves, (b) bar graph of σ_{FS} and m.

Table 2
Mechanical properties of different composites.

Specimen	Tensile property [28]			Fatigue property	
	YS (MPa)	UTS (MPa)	El (%)	σ_{FS} (MPa)	m
Uniform composite	671 ± 5	707 ± 5	2.5 ± 0.2	340	0.48
Bimodal-CG DZ	574 ± 5	680 ± 8	3.8 ± 0.5	300	0.44
Bimodal-UFG DZ	620 ± 7	720 ± 6	4.7 ± 0.5	320	0.44

3.4. Damage mechanism

In order to clarify the damage mechanism, the microhardness evolutions before and after fatigue were tested and the values are shown in Fig. 6. It can be seen that, the hardness of BZs was higher than that of DZs in the bimodal composites. Further, the hardness of the Uniform composite was slightly lower than that of BZs in the bimodal composites.

This was because that the higher CNT content in the BZs (with 3 vol% CNT) of bimodal composites led to their higher strengthen effect than that of the Uniform composite (with 2.25 vol% CNT). After fatigue, all the above microhardness was improved, which was mainly caused by the working-hardening. For a comparison, the improved hardness of BZs and DZs in the Bimodal-CG DZ was higher than that in the Bimodal-UFG DZ, which needs to be discussed after microstructure observation.

The TEM images of the Uniform composite after fatigue test are shown in Fig. 7. It can be found that the grains were still very small of approximately 200 nm and many CNTs (as red arrows indicated inside of Fig. 7a) pinning at the grain boundaries (GBs). According to the investigations on the metal materials' fatigue behaviors, UFGs would become larger during the fatigue loading, which could be owing to that the adjacent small grains tend to have the same orientation under repeated cyclic mechanical activation [41,42]. However, for the CNT/Al composites, the fine grains in the BZs kept stable after fatigue test, which
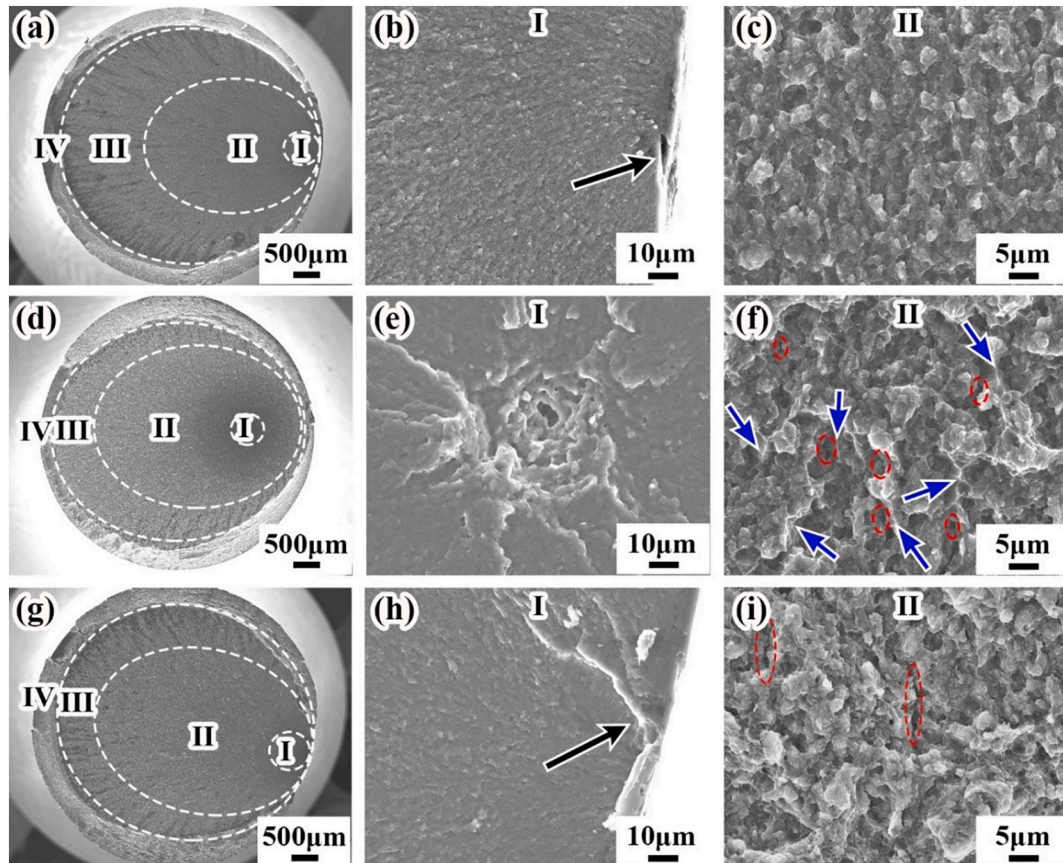
Fig. 5. Fracture morphologies for three different composites: (a)(b)(c) Uniform composite with the stress amplitude of 340 MPa after 1.3×10^6 cycles, (d)(e)(f) Bimodal-CG DZ with the stress amplitude of 310 MPa after 2.5×10^6 cycles, (g)(h)(i) Bimodal-UFG DZ with the stress amplitude of 330 MPa after 1.2×10^6 cycles.
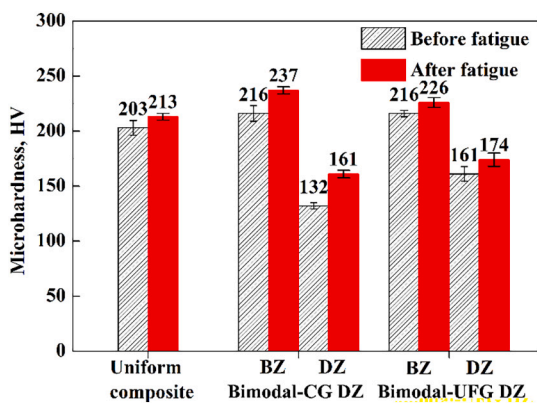
Fig. 6. Microhardness of the uniform and bimodal composites before and after fatigue test (for the fatigue samples, the Uniform, Bimodal-CG DZ and Bimodal-UFG DZ composites were respectively tested at the stress amplitude of 340 MPa with 1.3×10^6 cycles, 310 MPa with 2.5×10^6 cycles and 330 MPa with 1.2×10^6 cycles to failure).

was mainly because that the pinning effect of CNTs limited the change of grain orientation [43,44]. Further, the dislocation cells (as indicated by black arrows in Fig. 7b) were observed, and dislocation cell sizes were no larger than 200 nm. Dislocation cell as a typical fatigue characteristic had been found in many materials with high stacking fault energy, which was formed by dislocation slipping and reaction. Because the dislocation cells were mainly occurred inside of the grains, so the cell size was smaller than the grain size [45,46]. It should be mentioned that, the dislocation reaction would affect the material property evolution from the two aspects. On one hand, the new formed dislocations could promote the working-hardening, which would improve the hardness. On the other hand, the dynamic recovery, i.e., the formed dislocation cells would soften the material. As a result, the hardness improvement of the Uniform composite was weak.

The TEM images of the bimodal composites after fatigue test are shown in Fig. 8. For the Bimodal-CG DZ, no dislocation cells were observed within the BZs, but a small number of entangled dislocations inside the grains were observed (Fig. 8a). The microstructures within the DZs were quite different. Slip bands arranged parallel to each other were observed in the DZs (marked by blue arrows in Fig. 8b). This means that the deformation partition in the BZs was low with a weak dislocation reaction, and the deformation partition in the DZs was high with a severe dislocation reaction. The preferential deformation in the DZs decreased the deformation partition in the BZs agreed well with the

previous investigations on the bimodal Al alloys [23] and CNT/Al composites [28]. Because no obvious dislocation cells formed in the BZs, the soften effect was decreased, thereby leading to its higher hardness improvement of BZs in the Bimodal-CG DZ than that of the Uniform composite. The formation of slip bands within the DZs was the result of the directional movement of the dislocations on a specific slip plane, which indicates the local strain concentration in these zones [47,48]. The low strength of CG DZs and a large amount of deformation accumulated in the slip bands of DZs would worsen the fatigue performance of Bimodal-CG DZ. Therefore, the σ_{FS} and m of the Bimodal-CG DZ was lower than that of the Uniform composite.

For the Bimodal-UFG DZ, the dislocation cells were found within the BZs (Fig. 8c), which would decrease the working-hardening effect in these zones, therefore, the hardness improvement of the BZs in the Bimodal-UFG DZ was lower than that in the Bimodal-CG DZ. When observing the DZs of the Bimodal-UFG DZ, about 500 nm dislocation cells (as indicated by black arrows in Fig. 8d) could be seen. Different from that of the DZs in the Bimodal-CG DZ, there were no slip bands within the Bimodal-UFG DZ. This can be explained to that the grains in the DZs of the Bimodal-UFG DZ were refined and the abundant GBs inhibited the long-range directional slipping of dislocations [14]. The strength improvement in the DZs and disappearance of slip bands would decrease the stress concentration at the DZs. Therefore, the σ_{FS} of the Bimodal-UFG DZ was higher than that of the Bimodal-CG DZ.

According to our previous investigations on the tension-tension fatigue behaviors of bimodal CNT/Al composites, the refined grains in the DZs were good for improving the strength of the DZs, which would optimize the uncoordinated deformation between the BZs and DZs. At the same time, the dislocation piling up effect at the GBs of the BZs was weaken, which was owing to the stress relieving effect from the bimodal structure [28]. Finally, the Bimodal-UFG DZ even had the higher σ_{FS} than that of the Uniform composite. However, for the tension-compression fatigue at the present investigation, the σ_{FS} of the Bimodal-UFG DZ was lower than that of the Uniform composite, which could be owing to that the larger stress amplitude at tension-compression fatigue leading to more severe intragranular deformation, and the positive effect of bimodal structures on dislocation relaxation at BZs is not enough to offset the deterioration effect of large dislocation cells in the DZs.

Overall, the tension-compression fatigue behaviors of CNT/Al-Cu-Mg composites with uniform and bimodal structures can be summarized, and the schematic diagram of microstructure evolution after fatigue is shown in Fig. 9. For the Uniform composite, CNTs had a strong pinning effect on grain boundaries, which could keep the grains stable. With the cyclic loading, the dislocation cells within the grains formed.
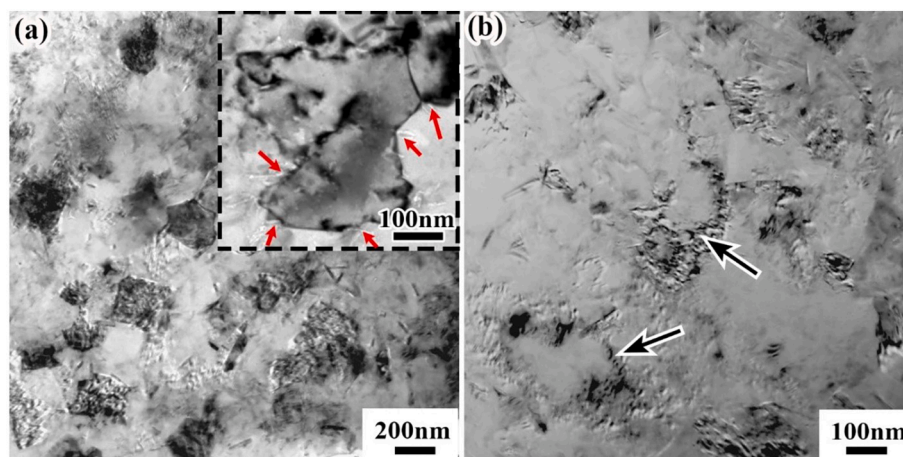
Fig. 7. TEM images of the Uniform composite with the stress amplitude of 340 MPa after 1.3×10^6 cycles: (a) grain and CNT distribution, (b) dislocation morphology.
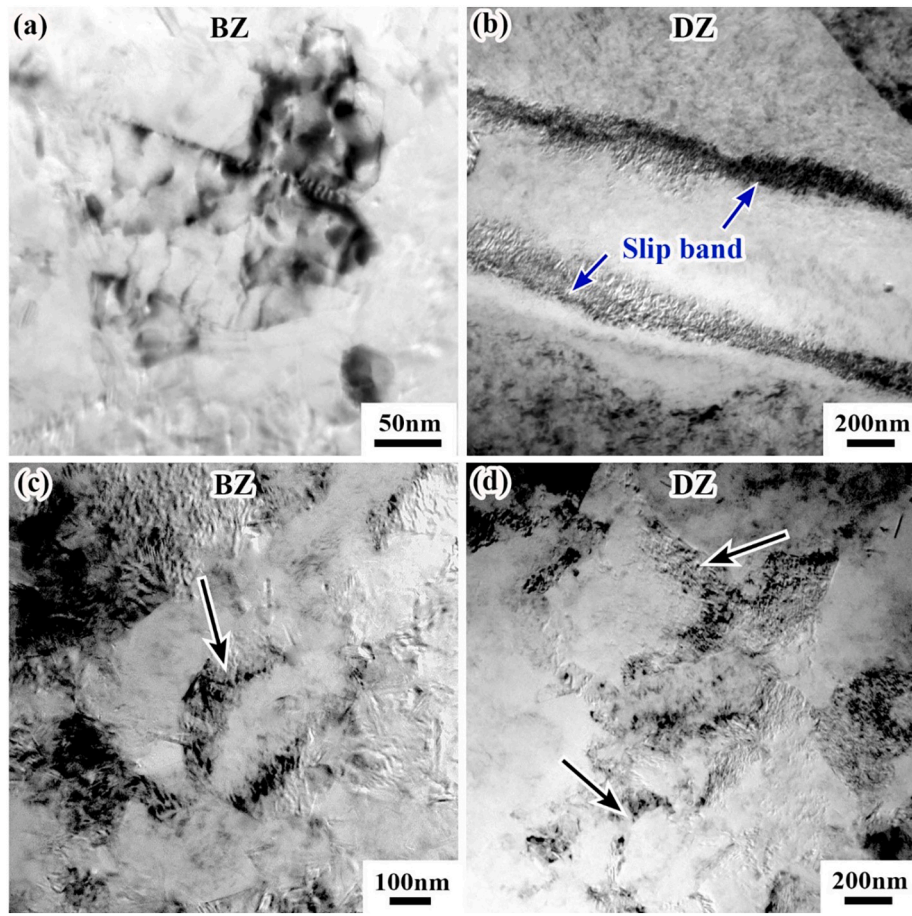
Fig. 8. TEM images of the microstructure for the two bimodal composites after fatigue test: (a)(b) Bimodal-CG DZ (with the stress amplitude of 310 MPa after 2.5 × 10^6 cycles), (c)(d) Bimodal-UFG DZ (with the stress amplitude of 330 MPa after 1.2 × 10^6 cycles).

The small grains in the Uniform composite led to the dislocation cells very small, which was good for its high fatigue strength. For the bimodal composites, the uneven deformation caused by bimodal structures would decrease the fatigue life. Especially, as the DZs had the grains larger than 1 μm, the slip bands inside the DZs formed, which caused the severe local deformation in the DZs, thereby accelerating the fatigue damage and leading to lower σ_{FS} and m. By appropriately refining grain size of the DZs to sub-micron level, the slip bands could be effectively avoided. Although the σ_{FS} of the bimodal composite with UFG DZs was still a little lower than that of the composite with the uniform structure, the σ_{FS} had been improved as compared the bimodal composite with CG DZs.

4. Conclusions

1) The pinning effect of CNTs on the grain boundaries could keep the grain stable after the fatigue loading. For the uniform composite, the uniform small grains also limited the size of dislocation cells to no larger than 200 nm, and because there was no formation of large dislocation configuration, the uniform composite exhibited excellent fatigue properties.

2) The fatigue cracks of the uniform composite and the bimodal composite with ultra-fine grained DZs originated from the specimen surface. The fatigue crack initiation of the bimodal composite with coarse grained DZs was more inclined to the inside of the specimen.
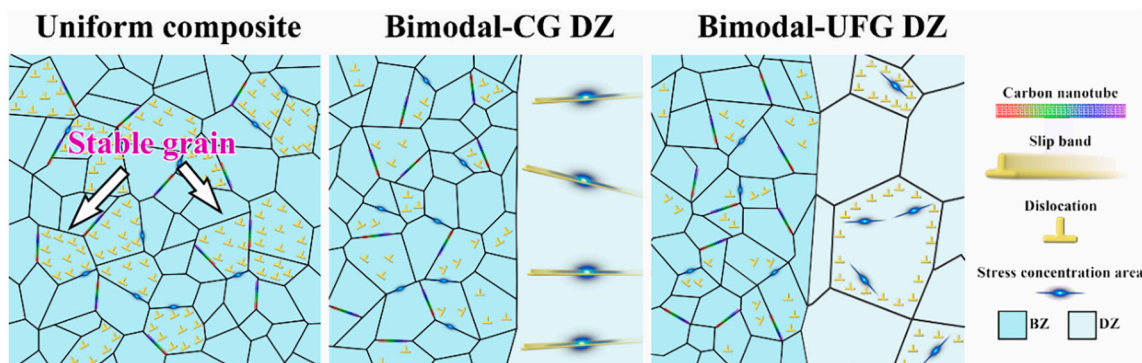
Fig. 9. Schematic diagram of microstructure evolution after tension-compression fatigue.

3) Slip bands formed within the coarse grained DZs of the bimodal composite during the fatigue test, which caused severe strain concentration and accelerated the progress of fatigue damage. By appropriately refining the grains of the DZs to sub-micron level, the slip bands could be avoided, which was good for improving the fatigue performance and maintain a high elongation.

Declaration of Competing Interest

The authors declared that they have no conflicts of interest to this work. We declare that we do not have any commercial or associative interest that represents a conflict of interest in connection with the work submitted.

Data availability

The data that has been used is confidential.

Appendix A. Supplementary data

Supplementary data to this article can be found online at https://doi.org/10.1016/j.matchar.2022.112193.

References

[1] X. Yang, T. Zou, C. Shi, E. Liu, C. He, N. Zhao, Effect of carbon nanotube (CNT) content on the properties of in-situ synthesis CNT reinforced Al composites, Mater. Sci. Eng. A 660 (2016) 11–18.

[2] X. Zhang, N. Zhao, C. He, The superior mechanical and physical properties of nanocarbon reinforced bulk composites achieved by architecture design – a review, Prog. Mater. Sci. 113 (2020), 100672.

[3] B. Chen, K. Kondoh, J. Li, M. Qian, Extraordinary reinforcing effect of carbon nanotubes in aluminium matrix composites assisted by in-situ alumina nanoparticles, Compos. Part B 183 (2020), 107691.

[4] Z.Y. Liu, B.L. Xiao, W.G. Wang, Z.Y. Ma, Analysis of carbon nanotube shortening and composite strengthening in carbon nanotube/aluminum composites fabricated by multi-pass friction stir processing, Carbon 69 (2014) 264–274.

[5] Z.Y. Liu, B.L. Xiao, W.G. Wang, Z.Y. Ma, Modelling of carbon nanotube dispersion and strengthening mechanisms in Al matrix composites prepared by high energy ball milling-powder metallurgy method, Composites Part A 94 (2017) 189–198.

[6] L. Jiang, Z. Li, G. Fan, L. Cao, D. Zhang, The use of flake powder metallurgy to produce carbon nanotube (CNT)/aluminum composites with a homogenous CNT distribution, Carbon 50 (2012) 1993–1998.

[7] S.C. Tjong, Recent progress in the development and properties of novel metal matrix nanocomposites reinforced with carbon nanotubes and graphene nanosheets, Mater. Sci. Eng. R 74 (2013) 281–350.

[8] S. Saadallah, A. Cable, S. Hamamda, K. Chetehouna, M. Sahli, A. Boubertakh, S. Revo, N. Gascoin, Structural and thermal characterization of multiwall carbon nanotubes (MWCNTs)/aluminum (Al) nanocomposites, Composites Part B-Engineering 151 (2018) 232–236.

[9] S. Bi, Z.Y. Liu, B.L. Xiao, Y.N. Zan, D. Wang, Q.Z. Wang, Z.Y. Ma, Enhancing strength-ductility synergy of carbon nanotube/7055Al composite via a texture design by hot-rolling, Mater. Sci. Eng. A 806 (2021), 140830.

[10] K. Ma, Z. Liu, X. Zhang, B. Xiao, Z. Ma, Fabrication of high strength carbon nanotube/7055Al composite by powder metallurgy combined with subsequent hot extrusion, SCIENCE CHINA Technol. Sci. 64 (2021) 1081–1091.

[11] S. Dong, J. Zhou, D. Hui, Y. Wang, S. Zhang, Size dependent strengthening mechanisms in carbon nanotube reinforced metal matrix composites, Composites Part A 68 (2015) 356–364.

[12] Z.Y. Liu, K. Ma, G.H. Fan, K. Zhao, J.F. Zhang, B.L. Xiao, Z.Y. Ma, Enhancement of the strength-ductility relationship for carbon nanotube/Al–Cu–Mg nanocomposites by material parameter optimisation, Carbon 157 (2020) 602–613.

[13] E.I. Salama, A. Abbas, A.M.K. Esawi, Preparation and properties of dual-matrix carbon nanotube-reinforced aluminum composites, Composites Part A 99 (2017) 84–93.

[14] K. Ma, Z.Y. Liu, K. Liu, X.G. Chen, B.L. Xiao, Z.Y. Ma, Structure optimization for improving the strength and ductility of heterogeneous carbon nanotube/Al–Cu–Mg composites, Carbon 178 (2021) 190–201.

[15] K. Ma, Z.Y. Liu, B.S. Liu, B.L. Xiao, Z.Y. Ma, Improving ductility of bimodal carbon nanotube/2009Al composites by optimizing coarse grain microstructure via hot extrusion, Composites Part A 140 (2021), 106198.

[16] X. Fu, Z. Tan, X. Min, Z. Li, Z. Yue, G. Fan, D.-B. Xiong, Z. Li, Trimodal grain structure enables high-strength CNT/Al-Cu-Mg composites higher ductility by powder assembly & alloying, Mater. Res. Lett. 9 (2021) 50–57.

[17] R. Shu, X. Jiang, H. Sun, Z. Shao, T. Song, Z. Luo, Recent researches of the bio-inspired nano-carbon reinforced metal matrix composites, Composites Part A 131 (2020), 105816.

[18] P. Xiao, Y. Gao, C. Yang, Y. Li, X. Huang, Q. Liu, S. Zhao, F. Xu, M. Gupta, Strengthening and toughening mechanisms of Mg matrix composites reinforced with specific spatial arrangement of in-situ TiB2 nanoparticles, Compos. Part B 198 (2020), 108174.

[19] J. Llorca, Fatigue of particle-and whisker-reinforced metal-matrix composites, Prog. Mater. Sci. 47 (2002) 283–353.

[20] A. Misra, H. Kung, D. Hammon, R.G. Hoagland, M. Nastasi, Damage mechanisms in nanolayered metallic composites, Int. J. Damage Mech. 12 (2003) 365–376.

[21] P.S. Pao, H.N. Jones, C.R. Feng, Fatigue crack growth and fracture toughness in bimodal Al 5083, mechanical properties of nanostructured materials and nanocomposites, December 1, 2003 - December 5, 2003, in: Materials Research Society, Boston, MA., United States, 2003, pp. 17–22.

[22] R. Liu, Y.Z. Tian, Z.J. Zhang, P. Zhang, Z.F. Zhang, Fatigue strength plateau induced by microstructure inhomogeneity, Mater. Sci. Eng. A 702 (2017) 259–264.

[23] S. Nelson, L. Ladani, T. Topping, E. Lavernia, Fatigue and monotonic loading crack nucleation and propagation in bimodal grain size aluminum alloy, Acta Mater. 59 (2011) 3550–3570.

[24] U. Krupp, H. Knobbe, H.-J. Christ, P. Koster, C.-P. Fritzen, The significance of microstructural barriers during fatigue of a duplex steel in the high- and very-high-cycle-fatigue (HCF/VHCF) regime, Int. J. Fatigue 32 (2010) 914–920.

[25] T. Qian, I. Karaman, M. Marx, Mechanical properties of nanocrystalline and ultrafine-grained nickel with bimodal microstructure, Adv. Eng. Mater. 16 (2014) 1323–1339.

[26] J. Long, Q. Pan, N. Tao, M. Dao, S. Suresh, L. Lu, Improved fatigue resistance of gradient nanograined Cu, Acta Mater. 166 (2019) 56–66.

[27] C. Shao, P. Zhang, X. Wang, Q. Wang, Z. Zhang, High-cycle fatigue behavior of TWIP steel with graded grains: breaking the rule of mixture, Mater. Res. Lett. 7 (2019) 26–32.

[28] K. Ma, X.N. Li, K. Liu, X.G. Chen, Z.Y. Liu, B.L. Xiao, Z.Y. Ma, Improving the high-cycle fatigue strength of heterogeneous carbon nanotube/Al-Cu-Mg composites through grain size design in ductile-zones, Compos. Part B 222 (2021), 109094.

[29] R.J. Morrissey, D.L. McDowell, T. Nicholas, Frequency and stress ratio effects in high cycle fatigue of Ti-6Al-4V, Int. J. Fatigue 21 (1999) 679–685.

[30] H.Z. Ding, O. Hartmann, H. Biermann, H. Mughrabi, Modelling low-cycle fatigue life of particulate-reinforced metal-matrix composites, Mater. Sci. Eng. A 333 (2002) 295–305.

[31] E.K. Gamstedt, B.A. Sjögren, Micromechanisms in tension-compression fatigue of composite laminates containing transverse plies, Compos. Sci. Technol. 59 (1999) 167–178.

[32] D. Pradhan, G.S. Mahobia, K. Chattopadhyay, D.C. Fernando, N. Paulose, S.N. N. Babu, V. Singh, Effect of stress ratio and mean stress on high cycle fatigue behavior of the superalloy IN718 at elevated temperatures, Materials Research Express 6 (2019) 10.

[33] X.L. Liu, C.Q. Sun, Y.S. Hong, Effects of stress ratio on high-cycle and very-high-cycle fatigue behavior of a Ti-6Al-4V alloy, Mater. Sci. Eng. A 622 (2015) 228–235.

[34] S. Bi, Z.Y. Liu, B.L. Xiao, P. Xue, D. Wang, Q.Z. Wang, R. Ni, Z.Y. Ma, Different fatigue behavior between tension-tension and tension-compression of carbon nanotubes reinforced 7055 Al composite with bimodal structure, Carbon 184 (2021) 364–374.

[35] Y.L. Lee, J. Pan, R. Hathaway, M.E. Barkey, Fatigue Testing and Analysis: Theory and Practice, Mechanical Engineering vol. 126, 2004, p. 59.

[36] A. Fatemi, A. Plaseied, A.K. Khosrovaneh, D. Tanner, Application of bi-linear log–log S–N model to strain-controlled fatigue data of aluminum alloys and its effect on life predictions, Int. J. Fatigue 27 (2005) 1040–1050.

[37] S.E. Shin, D.H. Bae, Fatigue behavior of Al2024 alloy-matrix nanocomposites reinforced with multi-walled carbon nanotubes, Compos. Part B 134 (2018) 61–68.

[38] J. Pang, S. Li, Z. Wang, Z. Zhang, Relations between fatigue strength and other mechanical properties of metallic materials, Fatigue Fract. Eng. Mater. Struct. 37 (2014) 958–976.

[39] J.Z. Liao, M.J. Tan, E. Bayraktar, Tension-tension fatigue behaviour of carbon nanotube reinforced Aluminium composites, Mater. Sci. Forum 765 (2013) 563–567.

[40] V. Gaur, V. Doquet, E. Persent, C. Mareau, E. Roguet, J. Kittel, Surface versus internal fatigue crack initiation in steel: influence of mean stress, Int. J. Fatigue 82 (2016) 437–448.

[41] K.K. Yogesha, A. Joshi, R. Jayaganthan, Fatigue behavior of ultrafine-grained 5052 Al alloy processed through different rolling methods, J. Mater. Eng. Perform. 26 (2017) 2826–2836.

[42] R. Goswami, C.R. Feng, S.B. Qadri, C.S. Pande, Fatigue-assisted grain growth in Al alloys, Sci. Rep. 7 (2017) 1–7.

[43] D.D. Phuong, P.V. Trinh, N.V. An, N.V. Luan, P.N. Minh, R.K. Khisamov, K. S. Nazarov, L.R. Zubairov, R.R. Mulyukov, A.A. Nazarov, Effects of carbon nanotube content and annealing temperature on the hardness of CNT reinforced

aluminum nanocomposites processed by the high pressure torsion technique, J. Alloys Compd. 613 (2014) 68–73.

[44] K. Ma, Z.Y. Liu, X.X. Zhang, B.L. Xiao, Z.Y. Ma, Hot deformation behavior and microstructure evolution of carbon nanotube/7055Al composite, J. Alloys Compd. 854 (2021), 157275.

[45] P. Das, R. Jayaganthan, T. Chowdhury, I.V. Singh, Fatigue behaviour and crack growth rate of cryorolled Al 7075 alloy, Mater. Sci. Eng. A 528 (2011) 7124–7132.

[46] D. Singh, P.N. Rao, R. Jayaganthan, High cyclic fatigue behaviour of ultrafine grained Al 5083 alloy, Mater. Sci. Technol. 30 (2014) 1835–1842.

[47] M. Li, A. Goyal, V. Doquet, N. Ranc, J.P. Couzinie, Ultrafine versus coarse grained Al 5083 alloys: from low-cycle to very-high-cycle fatigue, Int. J. Fatigue 121 (2019) 84–97.

[48] C. Huang, Y. Zhao, S. Xin, W. Zhou, Q. Li, W. Zeng, C. Tan, High cycle fatigue behavior of Ti5Al5Mo5V3Cr1Zr titanium alloy with bimodal microstructure, J. Alloys Compd. 695 (2017) 1966–1975.